

Министерство образования и науки Российской Федерации
Федеральное государственное автономное образовательное учреждение
высшего образования
“Московский физико-технический институт
(государственный университет)“

Магистерская диссертация
К среднему профилю и формированию поляризации
радиопульсаров

Студент 028 гр. Акопян А.Л.

Научный руководитель:
д.ф-м.н., профессор Бескин В.С.

Москва, 2016

Contents

1	Introduction	3
2	Propagation theory	4
2.1	Hollow cone model	5
2.2	Propagation effects	6
2.3	Modified plasma density profile	10
2.4	Large toroidal field	11
3	Radius-to-frequency mapping	15
4	Anomalous directivity patterns	17
5	Central hump	18
6	Discussions and conclusion	19

1 Introduction

It is widely known that the most important observational characteristics that depend strongly on the inclination angle α between magnetic and rotational axes are its mean profile and the position angle of linear polarization *p.a.*. These two parameters provide the most basic ideas about the geometric properties of the directivity pattern. But they appear to be non-reliable to determine the inclination angle. In the first paper by Beskin & Philippov 2012 the method was proposed of taking into account the circular polarization as well. This method, based on Kravtsov-Orlov equations, allowed to determine the swing of Stokes parameters in the neutron star magnetosphere along the ray trajectory, depending on the local plasma parameters and magnetic field structure. Observations together with numerical simulation of the ray propagation in the magnetosphere allow us to determine the unknown parameters more accurately.

Remember that during almost fifty years of study from the very beginning in 1967, when the pulsars were first observed, the major understanding in neutron stars' magnetosphere structure and in the origin of their activity was achieved. However, some questions still remain unexplained. The mass M , the period P , and the breaking factor of the pulsar \dot{P} can be determined directly with a good accuracy, but, on the other hand, such important parameter as an inclination angle α can be found only via indirect measurements with a significant uncertainty. As this angle is the most important parameter in the construction of the pulsars' magnetosphere model, the certain determination of that angle is of a crucial issue.

This is the third stage dedicated to the study of polarization characteristics based on our quantitative theory of the radio waves propagation in the pulsar

magnetosphere. In the first paper by Beskin & Philippov 2012 theoretical aspects of the polarization formation was studied, and the numerical simulation method was proposed. It allowing us to obtain polarization characteristics plots, with various parameters taken into account. In the second paper by Beskin et al. 2015 the statistics of polarization characteristics from different pulsars was considered.

In this work we majorly approved the numerical method. First, our simulations allow to conduct an accurate radius-to-frequency mapping, analyzing the mean intensity, circular polarisation and position angle curves, depending on the radiation generation region (both the characteristic size and height). Second, we obtain some effects that were not reproduced in the previous simulations, but that can be found in the observation data. Using this method, we also study the influence of the strong toroidal magnetic field on polarization characteristics of the radiation. This sort of toroidal field can be the consequence of a strong asymmetric current, that are obtained in MHD numerical simulations in Philippov, Tchekhovskoy & Li 2014. At the end of the paper, we demonstrate the possibility to reproduce the profiles of pulsars with anomalous directivity pattern, that seem not to expose the standard O-X-O pattern.

2 Propagation theory

In this section we discuss some general assumptions about the radiation generation and propagation effects that we used for our calculations. We also discuss some important results, obtained before in the first paper by Beskin & Philippov 2012.

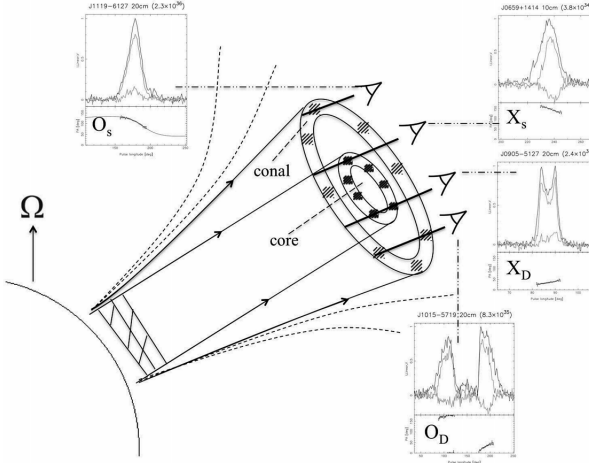


Figure 1: The schematic illustration of directivity pattern in hollow cone model.

2.1 Hollow cone model

For a long time it was known, that there are two radiation modes propagating in pulsars' magnetosphere: the extraordinary X-mode and the ordinary O-mode. While the X-mode propagates along the straight line without any refraction, the O-mode is being deflected in the region of strong magnetic field the star surface. This brought to an idea of the hollow-cone model for the directivity pattern generation, where there is an inner cone - straightly propagating X-mode, and the outer one is the O-mode that is deflecting from the magnetic axis. The radiation in the central region of the cone is suppressed due to large curvature radius of the magnetic field lines, as well as outside the edges of the polar cap region, where there are no open field lines. Various pulsar profiles correspond to different intersections of the line of sight and the directivity patter from the hollow-cone model (see Fig. 1).

Hollow cone model assumes the magnetic field to be dipole with the radiation propagating along a straight line. The polarization itself forms exactly in the same region, where the radiation generates, i.e., deep near star surface.

This assumptions allow us to analytically calculate the so-called RVM-curve for the *p.a.* plot along the rotation phase ϕ , studied in the paper by Radhakrishnan & Cooke 1969,

$$p.a. = \arctan \left(\frac{\sin \alpha \sin \phi}{\sin \alpha \cos \zeta \cos \phi - \sin \zeta \cos \alpha} \right), \quad (1)$$

where ϕ is the rotation phase, and ζ is the angle between the rotation axis and the line of sight. The equation (1) can be obtained considering the linear polarization that rigidly follows the magnetic field direction.

2.2 Propagation effects

While the approach of neglecting the propagation effects in pulsar profile simulation can work for some pulsars, most of them, however, appear to poorly correspond to this simplified approach. First of all, the *p.a.* curves of some profiles appear to be shifted from the center of the profile (clearly breaking the RVM-curve) and some expose anomalous humps in the center (see, e.g., PSR J1022+1001 Dai 2008). This problem is usually solved by considering the so-called retardation/aberration effects (later R/A) and by the assumption that the radiation generates at some given heights (see, e.g., Blaskiewicz et al. 1991, Krzeszowski et al. 2009, Dyks 2008 and Mitra & Seiradakis 2004). The R/A allows to determine the shift of the *p.a.* curve as $\Delta\phi \approx 4r_{\text{em}}\Omega/c$ and hence deduce the radiation origin height r_{em} . The general agreement from this naive technique, which is in a good agreement with geometric conclusions, is that the radiation originates in the deep regions near $10 \div 100R$.

However, it is clear, that to address to this problem self-consistently, one must take into account the effects of the ray propagation in the magnetosphere.

On the other hand, the profiles expose a nontrivial circular polarization, and this fact cannot be understood without the propagation effects.

In the paper by Andrianov & Beskin 2010 the importance of the propagation effects are shown. First of all, the refraction of the O-mode takes place in the region below the r_0 , where

$$r_0 \sim 10^2 R \cdot \lambda_4^{1/3} \gamma_{100}^{1/3} B_{12}^{1/3} \nu_{\text{GHz}}^{-2/3} P^{-1/5}. \quad (2)$$

Here and below R is the star radius, λ_4 is the multiplicity normalized by 10⁴, γ_{100} is the characteristic Lorentz-factor of secondary plasma normalized by 100, B_{12} is the surface magnetic field in 10¹² G, ν_{GHz} is the frequency in GHz and P is the period of rotation in seconds.

On the other hand, the polarization freezes far away from the neutron star surface (limiting polarization, see Zhelezniakov 1977), at $r < r_{\text{esc}}$, with

$$r_{\text{esc}} \sim 10^3 R \cdot \lambda_4^{2/5} \gamma_{100}^{-6/5} B_{12}^{2/5} \nu_{\text{GHz}}^{-2/5} P^{-1/5}. \quad (3)$$

In $r \sim r_{\text{esc}}$ the ray transits from the region of the dense plasma to the region of rarefied plasma. Thus one should consider the evolution of polarization characteristics from the region of generation up to r_{esc} , which for pulsars with ordinary parameters is much larger than the star radius.

The numerical approach with the method of Kravtsov-Orlov equation was proposed (see Kravtsov & Orlov 1990) that described the evolution of polarization characteristics along the line of sight

$$\frac{d\Theta}{dl} = \kappa + \frac{i\omega}{4c} [2\chi_{\{xy\}} \cos 2\Theta - 2\chi_{[xy]} - \chi_{xx} - \chi_{yy}] \quad (4)$$

on complex angle $\Theta = \Theta_1 + i\Theta_2$, with Θ_1 being the *p.a.* and $\Theta_2 = 1/2 \tan^{-1} V/I$, where V/I is the relative level of circular polarization.

In (4) χ_{xy} is the anisotropic part of the dielectric tensor, i.e., $\varepsilon_{ij} = \varepsilon\delta_{ij} + \chi_{ij}$, lying in the frame of two \mathbf{x} and \mathbf{y} perpendicular vectors in the picture frame, where \mathbf{x} is along the projection of $\nabla\varepsilon$ to the picture plane, and $\kappa = 1/2(\mathbf{x} \cdot (\nabla \times \mathbf{x}) + \mathbf{y} \cdot (\nabla \times \mathbf{y}))$.

For small $\Theta_2 \ll 1$, i.e., when the polarization forms in the deep regions $r_{\text{esc}} \ll c/\Omega$, one can approximate the level of circular polarization from (4) as

$$\frac{V}{I} \propto \frac{d(\beta_B + \delta)/dl}{\cos[2(p.a. - \beta_B - \delta)]}, \quad (5)$$

where the angle β_B corresponds to the magnetic field direction in the picture plane and δ is responsible for the drift contribution. Note, that if the propagation is neglected, we have the position angle following the direction of the magnetic field, i.e., $p.a. = \beta_B$. The important remark here is that for regions, where the drift contribution is not large enough, $\delta(r_{\text{esc}}) \ll 1$, the following relation occurs (see, e.g., Wang, Lai & Han 2010)

$$\frac{V}{I} \propto \frac{d\beta_B/dl}{\cos[2(p.a. - \beta_B)]} = \frac{\Omega/c(d p.a./d\phi)|_{r_{\text{esc}}}}{\cos[2(p.a. - \beta_B)]}, \quad (6)$$

so that the signs of V and $d p.a./d\phi$ are correlated. Namely, for X-mode the signs are the **same** ($p.a. \approx \beta_B$) and for the O-mode the signs are **opposite** ($p.a. \approx \beta_B + \pi/2$). Those results are reproduced in paper by Beskin & Philippov 2012.

The synchrotron absorption, that takes place near the region $r \sim r_{\text{abs}}$ where

$$r_{\text{abs}} = 2 \times 10^3 R \cdot \nu_{\text{GHz}}^{-1/3} \gamma_{100}^{-1/3} B_{12}^{1/3} \theta_{0.1}^{-2/3}. \quad (7)$$

Here $\theta_{0.1}$ is the characteristic angle between the propagation line and local magnetic field. In this region the equation $\omega_B = \tilde{\omega}\gamma\gamma_U$ is satisfied, and this resonance can be taken into account by multiplying the full intensity I_0 to the

integral optical density of the layer $I_\infty = I_0 e^{-\tau}$ (see, e.g., Luo & Melrose 2006 and Mikhailovskii et al. 1982)

$$\tau = \frac{2\omega}{c} \int_{r_{\text{em}}}^{>r_{\text{abs}}} \text{Im}[n] dl, \quad (8)$$

where r_{em} is the generation height and n is the refractive index, found by averaging the dielectric tensor over the plasma distribution function.

Moreover, in cases when $r_{\text{esc}} \gtrsim c/\Omega$ the dipole magnetic field should be adjusted to monopole wind component (see, e.g., Michel 1973 and Bogovalov 1999).

To summarize the most important results, obtained in Beskin & Philippov 2012, we can emphasize the following

- the strong suppression of the second peak in two-peaked profiles is observed, due to synchrotron absorption;
- the maximum of the *p.a.* derivative $(dp.a./d\phi)_{\text{max}}$, i.e., the center of the *p.a.* curve, shifts to the right relative to the center of the profile due to nonzero particle drift, which is also observed directly (see, e.g., Weltevrede & Johnston 2008: PSR J0729-1448, PSR J0742-2822, PSR J1105-6107 etc);
- it was shown that the value $(dp.a./d\phi)_{\text{max}}$, used to determine the values for the α angle (see, e.g., Kuzmin & Dagkesamanskaya 1983, Narayan & Vivekanand 1983, Malov 1990, Blaskiewicz et al. 1991 and Everett & Weisberg 2001), may drastically differ from that from the RVM model widely used.

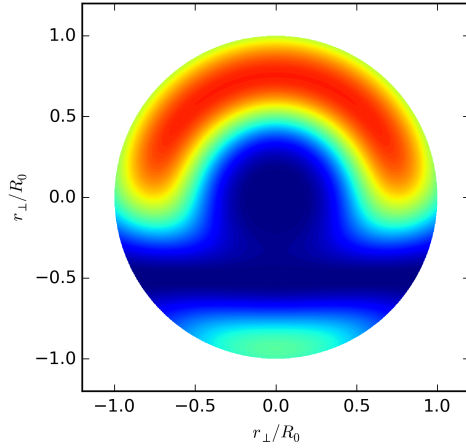


Figure 2: Density profile for angles $\alpha \approx 90^\circ$.

2.3 Modified plasma density profile

In this work we majorly improved our past approach taking into account new important effects.

Previously in paper Beskin & Philippov 2012 the symmetric polar cap was assumed. In general this assumption is incorrect and this fact may be important for large angles, for which the directivity pattern is crossing the $\Omega \cdot \mathbf{B} = 0$ line (where Goldreich-Julian density is suppressed $\rho_{GJ} = 0$). The old axisymmetric density profile is adjusted by the empiric gaussian factor, that depends on polar angle θ from the rotation axis Ω .

$$g(f) = \frac{\exp(-f^2)}{1 + (f_0/f)^{2.5}} \left(1 - \exp \left[-\frac{(90^\circ - \alpha - \theta)^2}{2(\delta\theta)^2} \right] \right), \quad (9)$$

where f is the dimensionless distance from the magnetic axis, and $\delta\theta$ is the empirical width of the $\Omega \cdot \mathbf{B} = 0$ gap (**REF TO ARZAMASSKIY & BE-SKIN**). The first term in (9) models the suppression of secondary plasma generation near the magnetic axes $f \lesssim f_0$, where the magnetic field lines have large curvature radius.

2.4 Large toroidal field

The two coupled equations describing the evolution of a pulsar are the following (Michel & Goldwire 1970)

$$\begin{aligned} I_r \dot{\Omega} &= -\frac{2}{3} \frac{B_0^2 R^6}{(c/\Omega)^3} \sin^2 \alpha, \\ I_r \Omega \dot{\alpha} &= -\frac{2}{3} \frac{B_0^2 R^6}{(c/\Omega)^3} \cos \alpha \sin \alpha, \end{aligned} \quad (10)$$

where the I_r is the moment of inertia of the pulsar with respect to the rotation axis and B_0 is the surface magnetic field. One can notice, that from (10) the following relation holds

$$\dot{\alpha} \propto -\frac{d}{d\alpha} |I_r \dot{\Omega}|, \quad (11)$$

which simply means, that the obliquity angle α evolves in such a way, that the total spindown energy losses are reduced (see Philippov, Tchekhovskoy & Li 2014).

It was obtained numerically that the spindown energy loss increases with the increasing α in 3D force-free simulations by Spitkovsky 2006, Kalapotharakos & Contopoulos 2009, Kalapotharakos et al. 2012 and Pétri 2012 with the further confirmation of the results in MHD simulations by Tchekhovskoy et al. 2013 and in PIC simulations by Philippov & Spitkovsky 2014. This implies the evidence for the evolution of the inclination angle α for oblique rotators towards zero, aligning the magnetic moment \mathbf{m} and rotation vector $\boldsymbol{\Omega}$.

On the other hand, the current outflow from the polar cap, that is ultimately responsible for the rotation energy loss (see, e.g., Beskin et al. 1983, Beskin et al. 1993 and Mestel et al. 1999), consists of two distinct components

$$i = i_S \cos \alpha + \frac{r_\perp}{r} i_A \sin \alpha, \quad (12)$$

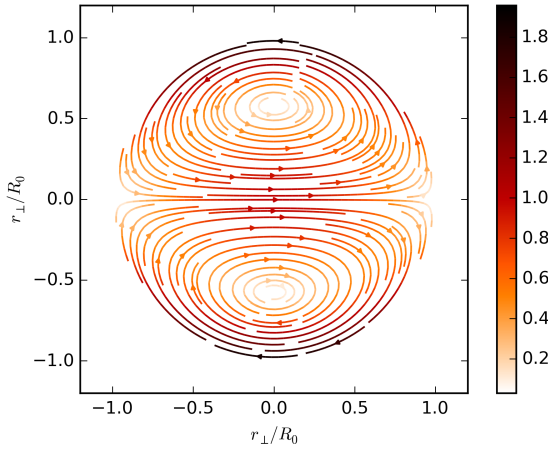


Figure 3: Toroidal magnetic field profile, generated by the large asymmetric current in units of $B_0 \frac{3}{4} \kappa \sin \alpha (R/r)^4$.

where i is the normalized to j_{GJ} current, i_S and i_A are the symmetric and antisymmetric components. In this terms one can deduce the angle evolution equation which in this case will be the following

$$\dot{\alpha} \propto - \left(\frac{\Omega R}{c} i_A + i_S \right). \quad (13)$$

Notice, that the contribution of asymmetric current is suppressed by the factor $\Omega R/c \ll 1$. To be consistent with the angle evolution described above, we should unavoidably imply the existence of a large asymmetric current $j_A/j_{\text{GJ}} \sim c/\Omega R \gg 1$. Recent studies of pair creation in the inner gap by Timokhin & Arons 2013 suggest that these large currents $j \gg j_{\text{GJ}}$ are indeed possible.

The toroidal magnetic field due to asymmetric current should in this case be taken into consideration as it may vastly contribute to polarization. This magnetic field in polar frame (r_\perp, φ) perpendicular to magnetic moment \mathbf{m} can

be written as

$$\begin{aligned} B_{r\perp} &= B_0 \frac{3}{4} \kappa \sin \alpha \frac{\left[(R_0/R)^2 - (r_\perp/R)^2 \right]}{(r/R)^4} \sin \varphi, \\ B_\varphi &= B_0 \frac{3}{4} \kappa \sin \alpha \frac{\left[(R_0/R)^2 - 3(r_\perp/R)^2 \right]}{(r/R)^4} \cos \varphi, \end{aligned} \quad (14)$$

where $R_0 = r\sqrt{r\Omega/c}$ is the radius of a "polar cap" on a distance r from the star surface and κ is an unknown arbitrary coefficient (see Fig. 3). Note that the equation (14) holds for $r_\perp < R_0$ which is the inner part of the cone and for the outer part the toroidal field is effectively zero because the asymmetric current flows only in the vicinity of the conal outflow region.

This large toroidal field decreases with the distance from the star with as

$$\frac{B_t}{B_0} \propto \kappa \sin \alpha \frac{R_0^2 R^2}{r^4} = \kappa \sin \alpha \left(\frac{r\Omega}{c} \right) \left(\frac{R}{r} \right)^2, \quad (15)$$

while the simple dipole magnetic field drops down as the third power of distance $B_d/B_0 \propto (R/r)^3$. So for the outer region above $r > r_t$

$$r_t \sim \sqrt{\frac{R\Omega}{c\kappa \sin \alpha}} \sim 70R \cdot P^{1/2} \kappa^{-1/2} \sin^{-1/2} \alpha \quad (16)$$

the polarization will mostly be determined by the toroidal magnetic field.

Ultimately, let us enumerate the important effects in terms of distances that are to be taken into account (see Fig. 4).

- The radiation will originate at some arbitrary height r_{em} , which in our case will be an open parameter.
- For $r < r_0$ (2) the refraction of O-mode takes place. As for the pulsars with average parameters $r_0 \sim 20 \div 50R$, the refraction plays role only for

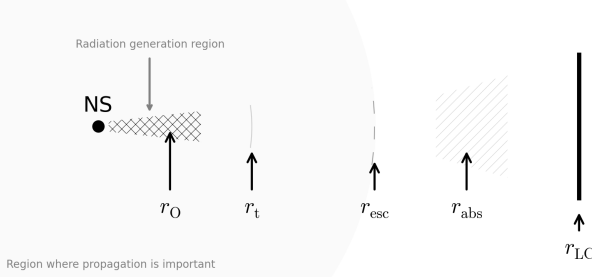


Figure 4: Schematic illustration of important height scales in the magnetosphere.

the central part of the profile, for which the propagation is nearly along the magnetic field lines and thus the refraction contribution should be negligibly small. On the other hand, for the conal radiation, i.e., the edges of the profile, for which the radiation originates high enough $r > r_O$, the refraction should be suppressed.

- If the large toroidal field is present, then from $r > r_t$ (16) the polarization characteristics should be majorly dictated by it.
- At some given region near $r \sim r_{\text{abs}}$ (7) the cyclotron resonance takes place, providing an effective opacity.
- The polarization evolves until the region of limiting polarization $r \sim r_{\text{esc}}$ (3), and to reproduce it correctly, one should integrate the Kravtsov-Orlov system (4) at least until this height.
- For most of the pulsars the light cylinder $r_{\text{LC}} = c/\Omega$ is rather high and polarization usually forms before reaching this region, i.e., $r_{\text{esc}} < r_{\text{LC}}$. However for millisecond pulsars or for pulsars with high plasma multiplicity λ the limiting polarization region r_{esc} can be comparable or even exceed

r_{LC} . In this case it is important to take into account the split-monopole component of the magnetic field.

3 Radius-to-frequency mapping

Understanding the size and depth of the region where the radio emission originates is a crucial point towards a construction of a self consistent radiation theory. Although there are no direct methods of determining the place of that region, there are several naive approaches that may help to do rough estimations. Namely, the A/R effects (Blaskiewicz et al. 1991, Krzeszowski et al. 2009) and geometric methods allowed to estimate that the radiation can originate in the region from $10 \div 100R$. However this approach fails if the propagation effects are large.

In this work we propose a method of conducting the radius-to-frequency mapping that allows to approximately determine the height and characteristic depth of the radiation region using polarization characteristics. To do that, we compare our simulation results of the *p.a.* with the corresponding observational plots. In Hankins & Rankin 2010 the *p.a.* curve has a characteristic scatter width that can be explained, if we assume that the radiation originates not from one particular radius, but rather from a wide shell.

The geometry of the pulsar, i.e., the inclination angle α and the angle to the observer β , as well as the approximate multiplicity λ , the characteristic gamma-factor γ_0 and the radiation height r_{em} can be determined from the mean profile and circular polarization level. After that we are left with only one parameter: Δr_{em} - the characteristic depth of that region.

We present the results of such analysis for the two-peaked pulsar PSR

B0301+19 (see Fig. 5) compared to the observational curves (see Fig. 6).

We approximated the scatter curve with the following parameters

PSR B0301+19			
ν [MHz]	$\Delta p.a.$	r_{em} [R]	Δr_{em} [R]
430 MHz	40°	80	50
1414 MHz	30°	50	30

where $\Delta p.a.$ is the rough scatter dispersion of the position angle data points.

Moreover, as the characteristic profile width of the profile is slimmer for higher frequency, this clearly demonstrates that in this case the altitude is lower, which is due to the fact that higher frequencies are generated in the deep regions close to the polar cap.

Nearly the same effects can be seen for the single-peaked PSR B0540+23 on Fig. 7 (observational data is presented on Fig. 8). The estimated upper boundaries for the altitudes in this case are

PSR B0540+23			
ν [MHz]	$\Delta p.a.$	r_{em} [R]	Δr_{em} [R]
430 MHz	50°	70	80
1414 MHz	30°	40	30

Basically the same trend holds here: higher frequencies are generated on lower altitudes and have a narrower radiation region. This fact, however, does not appear to be universal as for some pulsars the higher frequencies may have a wider radiation region (that can be estimated from $\Delta p.a.$), while still originating from the deep altitudes (e.g., PSR B0943+10, PSR B1133+16, PSR B2020+28).

The other parameters of these two pulsars' simulations are presented in Appendix A.

This approach, together with the observational scatter data for $p.a.$ (such as in catalog by HR) provides a strong instrument for estimating the upper bounds for the radiation region altitudes.

4 Anomalous directivity patterns

The classical hollow-cone directivity pattern appears to be approximately correct for most of the pulsars (see, e.g., Beskin et al. 2015). Although there is no precise correspondence between the signs of V and $d p.a./d\phi$ for a given mode, as the particle drift can in some cases drastically change the picture and the equation (6) will not always hold, in most cases one can determine the radiation mode by polarization curves. The classical directivity pattern following right from the hollow cone model assumes, that we mostly expect the O-mode radiation on the edges of the profile and X-mode near the center, leading to profiles such as: "X", "X-X", "O", "O-O", "O-X-O".

However, some pulsars expose anomalous directivity pattern that poorly fit to that simplified model. Namely, PSR J2048-1616 has three peaks following the "X-O-X" pattern, or PSR J0738-4042 with the same "X-O-X", but with suppressed radiation in the edges (the pattern can be reconstructed from polarization data). The directivity pattern of those pulsars cannot be explained in terms of classical hollow cone model. However we show, that propagation effects can explain their anomalous behaviour.

In Fig. 9 and Fig. 10 the simulated profiles for PSR J2048-1616 and PSR J0738-4042. We model the radiation on two distinct widely separated

regions. The altitude parameters for both are roughly similar

PSR J2048-1616, PSR J2048-1616		
Mode	$r_{\text{em}} [R]$	$\Delta r_{\text{em}} [R]$
X-mode	100	40
O-mode	10	5

As one can see, the anomalous polarization profiles can be easily explained using this technique. However, it is important to note, that the absolute intensity from a given height is an open parameter that in this case was adjusted by hand to fit the profiles.

5 Central hump

As we mentioned above, some two-peaked pulsars demonstrate a strange *p.a.* behaviour at the central region (see Fig. 11 right). The difference of our *p.a.* curve from the standard rotation vector model curve (1) is as strong as the density of secondary plasma. Thus in the regions, where the plasma density is suppressed (central region of the hollow cone) our curve will tend to be closer to the RVM, resulting the hump in the center. This phenomena can as well be observed in some two-peaked profiles near the central region (see Weltevrede & Johnston 2008), however, due to suppression of radiation in that region, it is hard to detect the *p.a.* value there.

In Fig. 11 we demonstrate this effect in simulated two-peaked pulsar (left) in comparison with real observational data for PSR J1022+1001. This hump effect was previously explained by Mitra & Seiradakis 2004, where authors

assumed the radiation generating at various heights. We, however, show, that there is no need to assume an anomalous altitude profile for radiation.

6 Discussions and conclusion

In this work we demonstrated the possibility to simulate pulsar profiles taking into account various propagation effects. In section 2 we discussed the main theoretical assumptions. We argue, that it is of a great importance to take into account the propagation effects when studying the polarizational characteristics.

In section 3 we conducted the radius-to-frequency mapping for two characteristic pulsars, showing the possibility to determine the altitudes of the region, where the radiation originates. The altitudes are in a good agreement with the results conducted using the simple A/R and geometric effects in papers by Blaskiewicz et al. 1991 and Krzeszowski et al. 2009. But upon that, our method provides an information about the width of the radiating region.

In section 4 discussed the possible explanations for the anomalous directivity pattern of some pulsars. While most of the pulsars follow the simple hollow cone model directivity pattern, some clearly contradict with it. We show, that assuming the generation of X and O modes on various altitudes one can still easily explain that behaviour.

In section 5 we showed that there is no need to assume anomalous altitude profile of radiation for some two-peaked pulsars, that have a hump in the center of the profile (as done by Mitra & Seiradakis 2004). Such an effect can easily be explained by the suppression of the plasma density near the center, as in this case we will have a weaker shift from the RVM curve.

We assume that the further development of this self-consistent technique will allow to make a powerful instrument to study not only the distinct effects of polarization profiles, but to indirectly obtain the approximate plasma parameters of individual pulsars.

References

Andrianov A.S. & Beskin V.S., Astronomy Letters **36**, pp. 248-259 (2010).

Beskin V.S., Gurevich A.V., Istomin Ia.N., JETP **85**, pp. 401-433 (1983).

Beskin V.S., Gurevich A.V., Istomin Ia.N., *Physics of the Pulsar Magnetosphere*, 432 p. (1993).

Beskin V.S., Jaroenjittichai P., Kramer M., Philippov A.A., Mon. Not. R. Astron. Soc. ???, ??? (2015).

Beskin V.S. and Philippov A.A., Mon. Not. R. Astron. Soc. **425**, p. 814 (2012).

Blaskiewicz M., Cordes J. M., Wasserman I., Astrophysical Journal **370**, pp. 643-669 (1991).

Bogovalov S.V., Astronomy and Astrophysics **349**, pp. 1017-1026 (1999).

Dai S. et al., Mon. Not. R. Astron. Soc. **449**, pp. 3223-3262 (2008).

Dai S., Hobbs G., Manchester R.N. et al., Mon. Not. R. Astron. Soc. **449**, pp. 3223-3262 (2015).

Dyks J., Mon. Not. R. Astron. Soc. **391**, pp. 859-868 (2008).

Everett J.E., Weisberg J.M., Astrophysical Journal, **553**, pp. 341-357 (2001).

Gould D.M., Lyne A.G., Mon. Not. R. Astron. Soc. **301**, pp. 235-260 (1998).

Hankins T.H. & Rankin J.M., The Astronomical Journal **139**, pp. 168-175 (2010).

Kalapotharakos C. & Contopoulos I., *Astronomy and Astrophysics* **496**, pp. 495-502 (2009).

Kalapotharakos C., Contopoulos I., Kazanas D., *Mon. Not. R. Astron. Soc.* **420**, pp. 2793-2798 (2012).

Karastergiou A., Johnston S., *Mon. Not. R. Astron. Soc.* **365**, pp. 353-366 (2006).

Kuzmin A.D. & Dagkesamanskaya I.M., *Soviet Astronomy Letters* **9**, pp. 80-83 (1983).

Kravtsov Yu.A. & Orlov Yu.I., *Geometrical Optics of Inhomogeneous Media*, Springer, Berlin (1990).

Krzeszowski K., Mitra D., Gupta Y., Kijak J., Gil J. and Acharyya A., *Mon. Not. R. Astron. Soc.* **393**, pp. 1617-1624 (2009).

Luo Q. & Melrose D.B., *Mon. Not. R. Astron. Soc.* **325**, pp. 187-196 (2006).

Malov I.F., *Soviet Astronomy* **34**, p. 189 (1990).

Mestel L., Panagi P., Shibata S., *Mon. Not. R. Astron. Soc.* **309**, pp. 388-394 (1999).

Michel F.C., *Astrophysical Journal* **180**, pp. 207-226 (1973).

Michel F.C. & Goldwire H.C. Jr., *Astrophysical Letters*, **5**, p. 21 (1970).

Mikhailovskii A.B., Onishchenko O.G., Suramishvili G.I., Sharapov S.E., *Soviet Astronomy Letters* **8**, pp. 369-371 (1982).

Mitra D., Seiradakis J.H., *arXiv: astro-ph/0401335* (2004).

Narayan R., Vivekanand M., *Astrophysical Journal* **274**, pp. 771-775 (1983).

Pétri J., *Mon. Not. R. Astron. Soc.* **424**, pp. 605-619 (2012).

Philippov A.A., Spitkovsky A., *Astrophysical Journal* **785**, pp. 6 (2014).

Philippov A.A., Tchekhovskoy A., Li J.G., *Mon. Not. R. Astron. Soc.* **441**, p. 1879 (2014).

Radhakrishnan V., Cooke D. J., *Astrophysical Letters* **3**, p. 225 (1969).

Spitkovsky A., *The Astrophysical Journal* **648**, pp. L51-L54 (2006).

Tchekhovskoy A., Spitkovsky A., Li J.G., *Mon. Not. R. Astron. Soc. Letters* **435**, p. L1-L5 (2013).

Timokhin A.N., Arons J., *Mon. Not. R. Astron. Soc.* **429**, pp. 20-54 (2013).

Wang C., Lai D., Han J., *Mon. Not. R. Astron. Soc.* **403**, pp. 569-588 (2010).

Weltevrede P. and Johnston S., *Mon. Not. R. Astron. Soc.* **391**, p. 1210 (2008).

Zhelezniakov V.V., *Electromagnetic waves in space plasma*, 432 p. (1977).

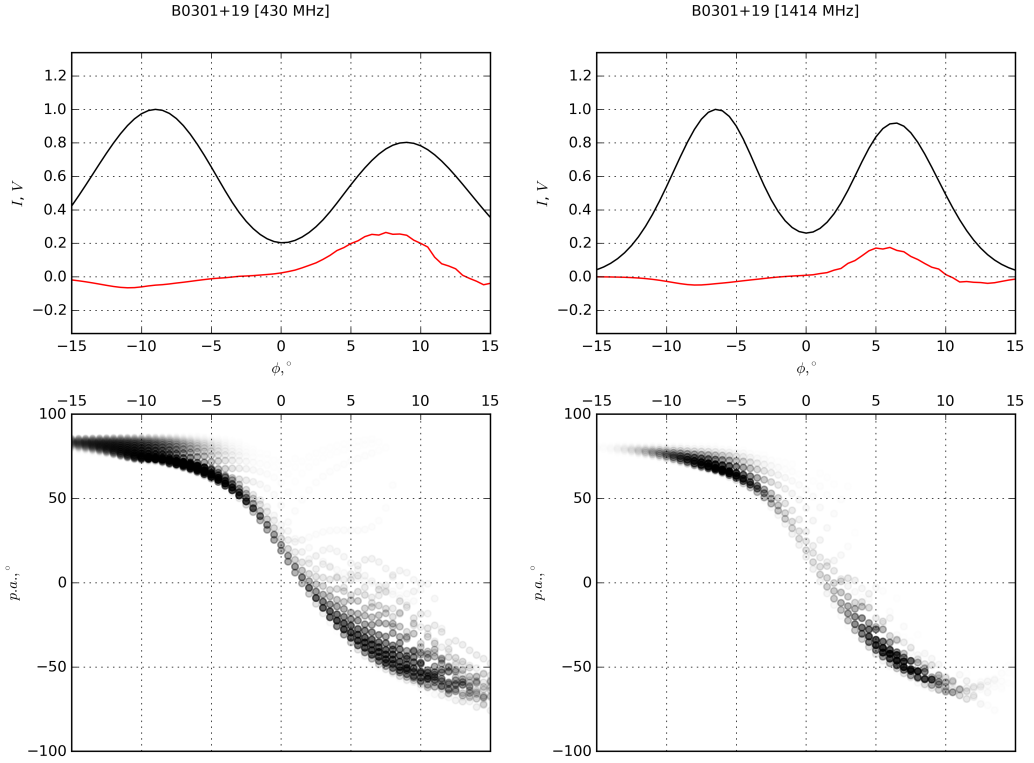


Figure 5: Simulated profiles for PSR B0301+19 at two distinct frequencies.

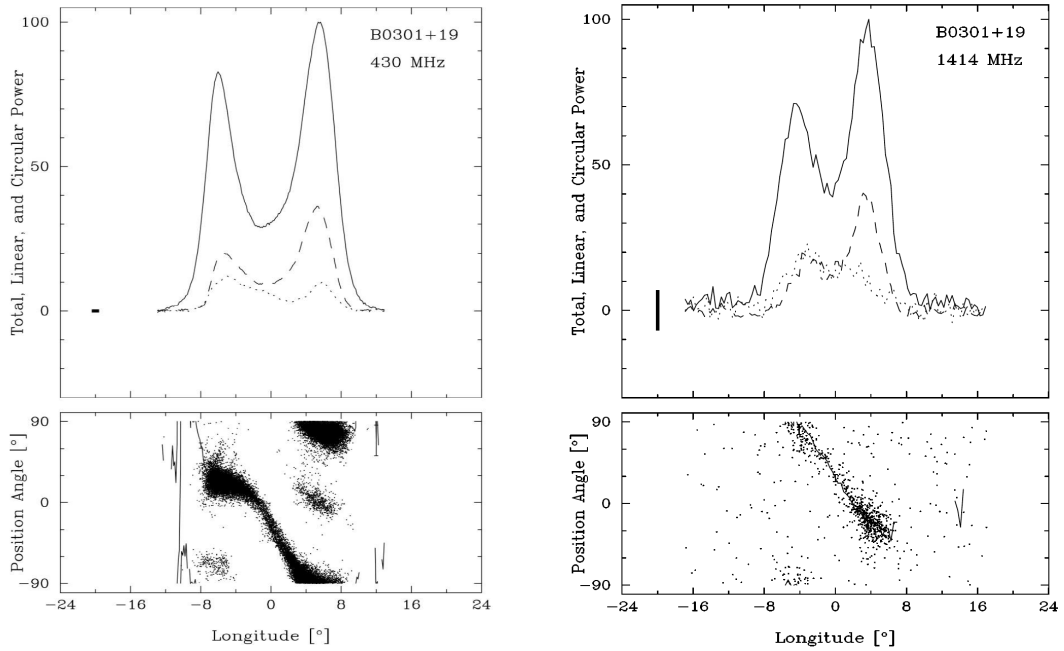


Figure 6: Observed profiles for PSR B0301+19 at two distinct frequencies (Hankins & Rankin 2010).

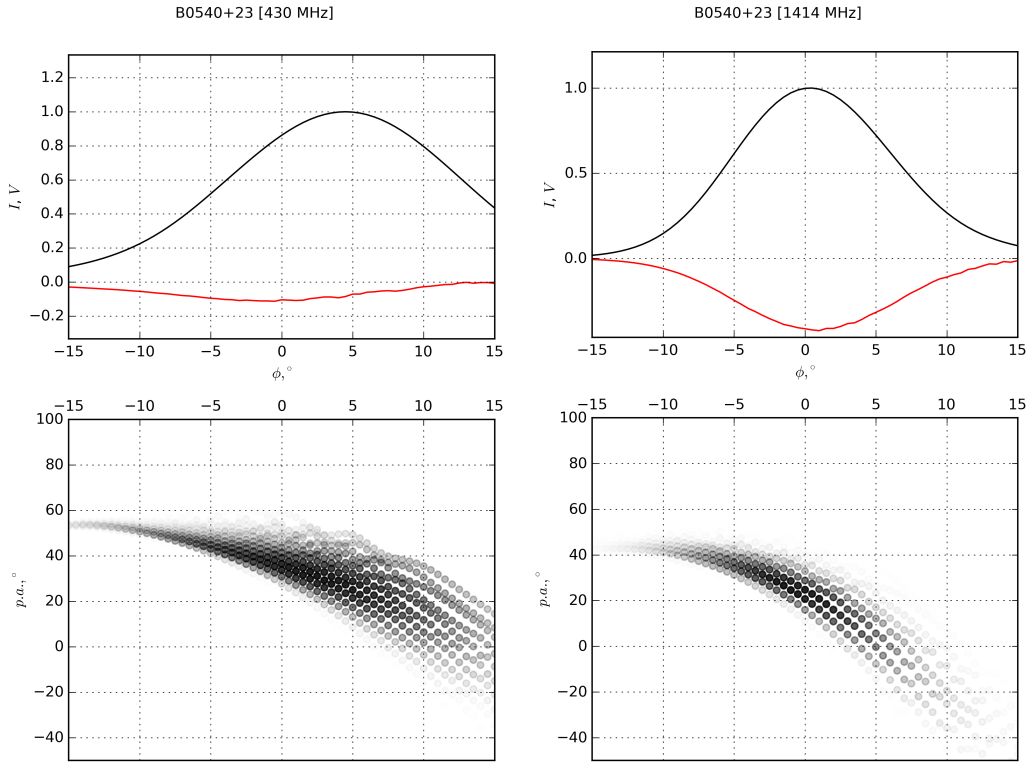


Figure 7: Simulated profiles for PSR B0540+23 at two distinct frequencies.

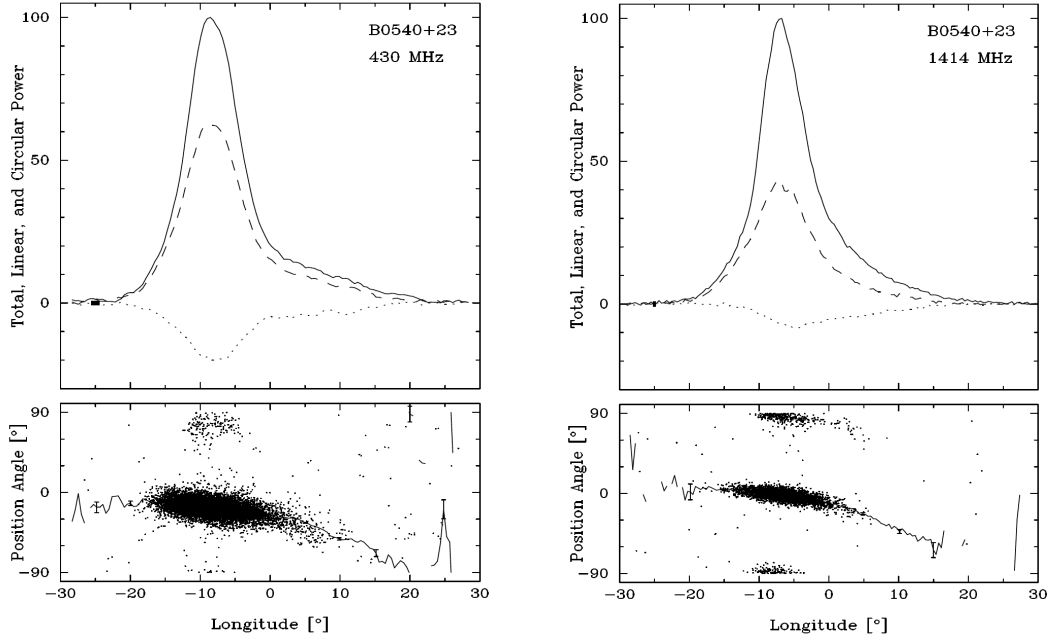


Figure 8: Observed profiles for PSR B0540+23 at two distinct frequencies (Hankins & Rankin 2010).

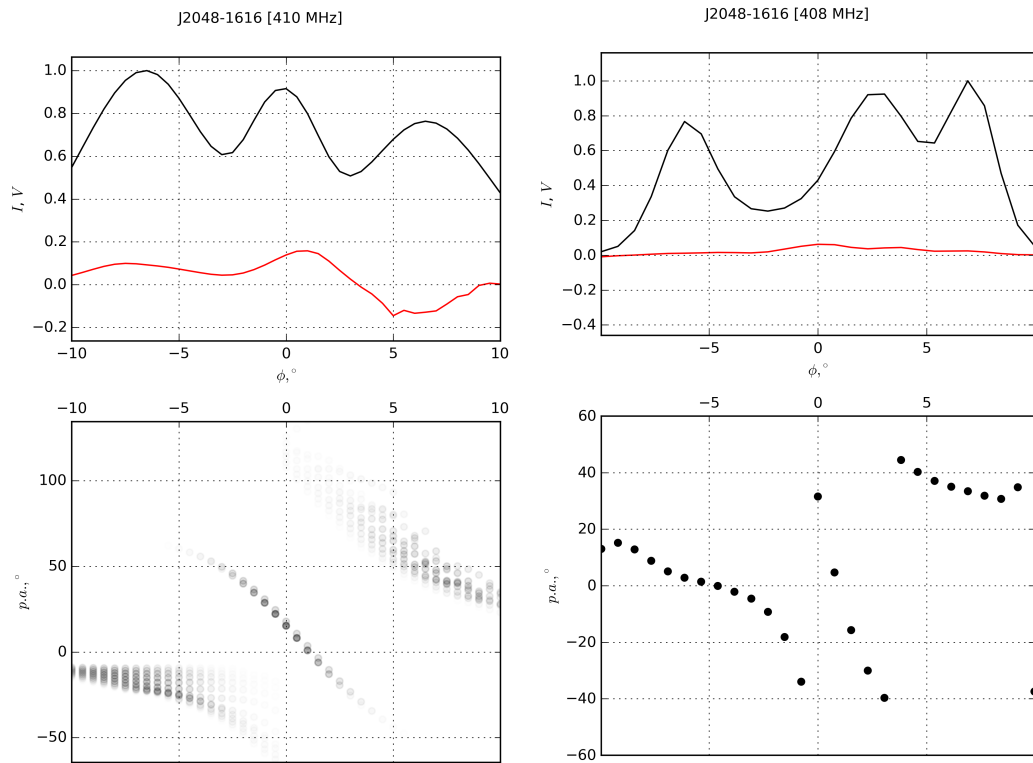


Figure 9: Simulated profile for PSR J2048-1616 at 410 MHz in comparison with observational data from Gould & Lyne 1998.

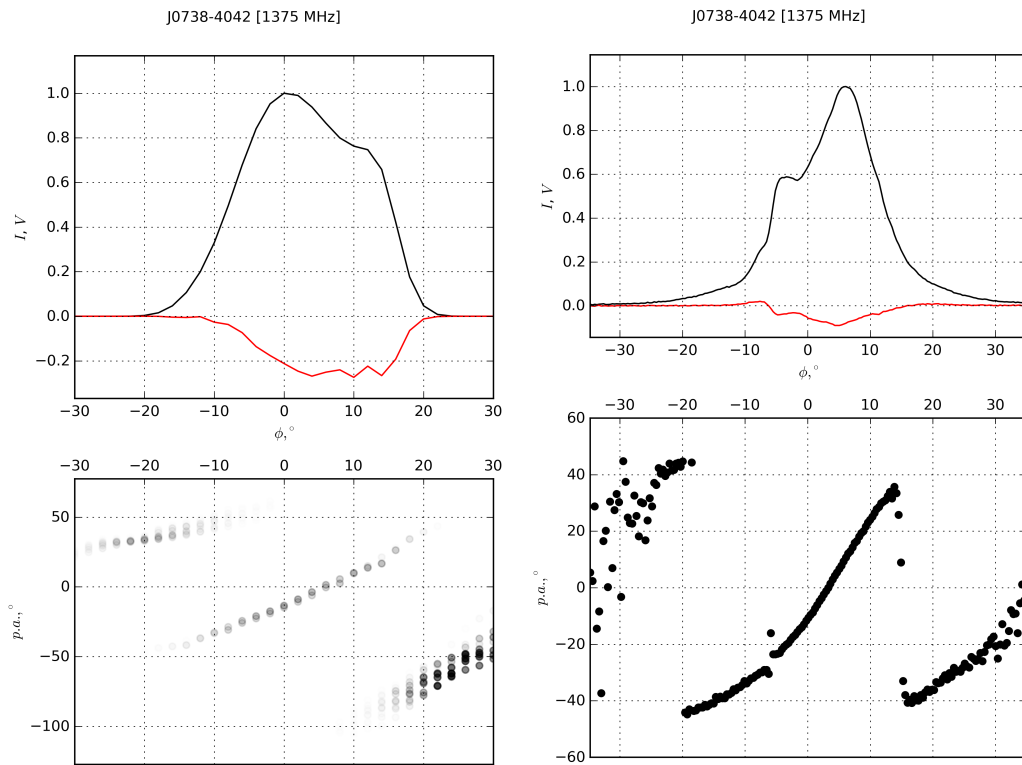


Figure 10: Simulated profile for PSR J0738-4042 at 410 MHz in comparison with observational data from Karastergiou & Johnston 2006.

J1022+1001 [728 MHz]

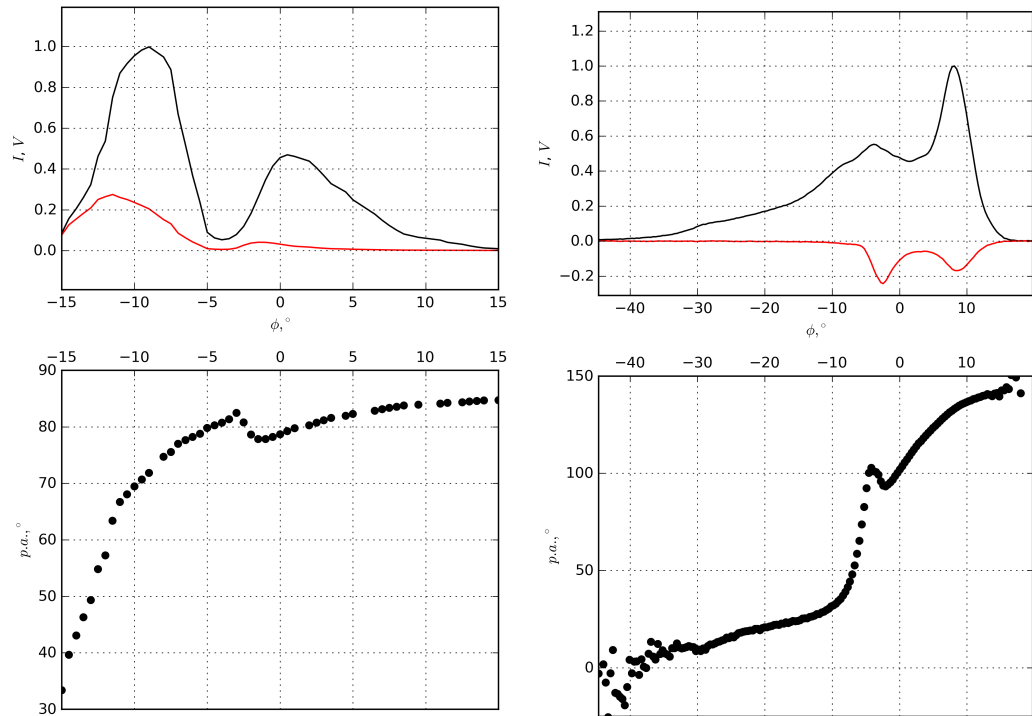


Figure 11: Simulated profile for PSR J1022-1001 at 728 MHz in comparison with observational data from Dai 2015.